A thermo-mechanically coupled cyclic plasticity model at large deformations considering inelastic heat generation

Qianhua Kan [1,*], Guozheng Kang [1], Wenyi Yan[2], Yilin Zhu [1], Han Jiang[1]

[1] Department of Applied Mechanics and Engineering, Southwest Jiaotong University, Chengdu, 610031, China

[2] Department of Mechanical and Aerospace Engineering, Monash University, Clayton, VIC3800, Australia

* Corresponding author: qianhuakan@yahoo.com.cn

Abstract In the process of inelastic deformation, cyclic accumulation of heat flux transferred from plastic work under cyclic loading results in an increased work temperature. The heat softening effects of material properties and external heat source will produce more plastic work. The fraction between plastic work and heat generation per unit volume can be introduced as a coupled source for thermal-mechanical analysis. Such coupling might be important in a simulation in which extensive inelastic deformation is accumulated fairly rapidly under cyclic loading and the mechanical properties are temperature dependent. To investigate the couple effect among temperature, stress and deformation under cyclic loading, a coupled thermo-mechanically cyclic plasticity model combined nonlinear isotropic hardening and kinematic hardening was established firstly in thermodynamics frame at large deformations. And then, the proposed model was implemented into finite element code ABAQUS by combining the user subroutine UMAT and UMATHT. Finally, some numerical results show the proposed model can capture thermal-induced necking in tensile loading, and the isotropic and kinematic hardening and thermal softening under cyclic loadings.

Keywords Inelastic heat generation, ratchetting, thermal softening, cyclic loading

1. Introduction

Elastic-plastic deformation behavior under cyclic loading has been investigated for some decades. Material models which describing macroscopic ratcheting response can be obtained within the framework of plasticity by combining the von Mises yield criterion with nonlinear kinematic hardening rules, e.g., the Armstrong-Frederick rule [1]. Some extended constitutive models of cyclic plasticity have been proposed to reasonably predict cyclic deformation behaviours of metal materials [2-6]. As a matter of fact, in the process of inelastic deformation, cyclic accumulation of heat flux transferred from plastic work under cyclic loading results in an increased work temperature. The thermal softening effect of material properties and external heat source will produce more plastic work The fraction between plastic work and heat generation per unit volume can be introduced as a source of coupling for thermal-mechanical analysis. However, the thermal effect induced by inelastic heat generation and its coupling with deformation were neglected in most ratcheting models. It is a reason that all the above-mentioned ratcheting models concern ratcheting in the context of small strains, the inelastic heat generation is neglectful small.

Recent experimental observation found that the ratchetting strain is up to 50% in the low-cycle fatigue [7], and thermo-elastic-plasticity coupling analysis in actual engineering application has attract attention [8]. So ratcheting problem without shakedown needs to be addressed on a consistent thermodynamic and large deformation frame. The thermo-mechanically coupled effect only in monotonic loading case has been modeled by the thermo-mechanically coupling constitutive models [9-16]. Therefore, a thermo-mechanically coupling cyclic plasticity constitutive model

needs to be established and make it available in commercial finite element packages, such as Abaqus for structural analysis.

In this work, a thermo-mechanically coupled cyclic plasticity model combined nonlinear isotropic hardening and kinematic hardening was established firstly in thermodynamics frame at large deformations. Further, the proposed model was implemented into finite element code ABAQUS by combining the user subroutine UMAT and UMATHT. Some numerical results were provided to validate the proposed model by simulating coupling thermo-mechanically behaviours under monotonic and cyclic loadings.

2. Thermo-elastic-plastic constitutive model

2.1. Deformation gradients

If the total deformation of materials is enough small, the thermal effect deriving from inelastic thermal generation is not significant. Therefore, the proposed model is derived at large deformation based on the hypoelastic-plastic theory. To separate recoverable and plastic contributions of the deformation gradient, the multiplicative decomposition of the deformation gradient is used [17]

$$\mathbf{F} = \mathbf{F}^r \mathbf{F}^p, \quad \mathbf{F}^r = \mathbf{F}^e \mathbf{F}^T \tag{1}$$

where $\mathbf{F}^r$ and $\mathbf{F}^p$ represents the thermo-elastic recoverable contribution and the plastic contribution of the total deformation gradient, respectively [18]. For metal materials, $\mathbf{F}^r$ describes the reversible distortion of the crystal, $\mathbf{F}^p$ describes irrecoverable deformation, for instance dislocation movements. Moreover, $\mathbf{F}^e$ and $\mathbf{F}^T$ are the elastic and thermal parts of the deformation gradient, respectively. For most metal materials, the elastic and thermal strains are small, and the multiplicative decomposition may be approximated by an additive decomposition of velocity gradient tensor $\mathbf{L}$ [16]

$$\mathbf{L} = \mathbf{L}^e + \mathbf{L}^T + \mathbf{L}^p \tag{2}$$

The rate of deformation tensor is the symmetrical part of velocity gradient tensor $\mathbf{L}$

$$\mathbf{D} = \frac{1}{2}(\mathbf{L} + \mathbf{L}^T) \tag{3}$$

2.2. Constitutive equations

Using the symmetric part of velocity gradient tensor in Eq. (2), the additive decomposition of the total rate of deformation tensor is expressed as

$$\mathbf{D} = \mathbf{D}^e + \mathbf{D}^p + \mathbf{D}^T \tag{4}$$

When we use the symmetric part of the velocity gradient with respect to current position and when the total elastic strain is always small compared to one. The rate of deformation decomposition is used in the form in almost all the inelastic constitutive models in finite element codes.

If only isotropic materials are considered, the elastic part of deformation rate can be given as

$$\mathbf{D}^e = \frac{1}{2G}\overset{\circ}{\tau} - \frac{v}{E}(tr\overset{\circ}{\tau})I \tag{5}$$

The thermal part of the rate of deformation tensor for isotropic materials can be expressed as

$$\mathbf{D}^T = \alpha \dot{T} \mathbf{I} \tag{6}$$

where α is thermal expansion coefficient and $\mathbf{I}$ is unit second order tensor.

At large deformation, an objective rate must be provided to state the objectivity of constitutive equations. The elastic stress-strain relation based on Jaumann objective rate can be written as

$$\overset{\circ}{\boldsymbol{\sigma}} = \mathbf{C}^e : \mathbf{D}^e = \mathbf{C}^e : (\mathbf{D} - \mathbf{D}^p - \mathbf{D}^T) \tag{7}$$

where $\overset{\circ}{\boldsymbol{\sigma}}$ is Jaumann rate of Cauchy stress, $\mathbf{C}^e$ is four order elastic tensor. Considering von Mises plasticity combined isotropic hardening and kinematic hardening and temperature dependent material properties, the yield function is expressed as a function of stress, temperature and equivalent plastic strain:

$$f = \bar{\sigma} - \sigma_y(\bar{\varepsilon}^p, T) \tag{8}$$

The equivalent stress can be defined as

$$\bar{\sigma} = \sqrt{1.5(\mathbf{s} - \boldsymbol{\alpha}) : (\mathbf{s} - \boldsymbol{\alpha})} \tag{9}$$

where $\boldsymbol{\alpha}$ is deviatoric back stress and the deviatoric part of stress tensor $\mathbf{s}$ is defined as

$$\mathbf{s} = \boldsymbol{\sigma} - \frac{1}{3} tr(\boldsymbol{\sigma}) \mathbf{I} \tag{10}$$

Associated plastic flow is used to derive the plastic part of deformation rate:

$$\mathbf{D}^p = \frac{\partial f(\mathbf{s} - \boldsymbol{\alpha})}{\partial \boldsymbol{\sigma}} \dot{\bar{\varepsilon}}^p = \dot{\bar{\varepsilon}}^p \mathbf{N} \tag{11}$$

where $\mathbf{N}$ is flow tensor of plastic strain and $\dot{\bar{\boldsymbol{\varepsilon}}}^p$ is the equivalent plastic rate defined as

$$\dot{\bar{\varepsilon}}^p = \sqrt{\frac{2}{3} \mathbf{D}^p : \mathbf{D}^p} \tag{12}$$

The isotropic hardening can be regarded as an increasing size in yield surface. In general, an exponential hardening is adopted to describe isotropic hardening with a threshold value as follows

$$\sigma_y(T) = \sigma_{y0}(T) + Q_{sa}(T)(1 - \exp(-b(T)\bar{\varepsilon}^p)) \tag{13}$$

where σ_{y0} is initial yield stress in the uniaxial loading at a reference temperature. The isotropic hardening parameters b and Q_{sa} are temperature dependent and can easily be calibrated by the uniaxial strain cycling at different temperatures.

A successful and popular approach is to introduce several back-stresses, where each back-stress is governed by the Armstrong-Frederick type of hardening rule. These models can be united in the following form:

$$\boldsymbol{\alpha}_i = \frac{2}{3} k_{1i}(T) \mathbf{D}^p - k_{2i}(T) \boldsymbol{\alpha}_i \dot{p}\,, \quad \boldsymbol{\alpha} = \sum_{i=1}^{M} \boldsymbol{\alpha}_i \tag{14}$$

where k_{1i} and k_{2i} are linear kinematic hardening coefficient and dynamics recovery coefficient for superposed M back stress components, respectively. Difference in Armstrong-Frederick typed models causes by different expressions in k_{1i} and k_{2i}. The accumulated plastic strain rate $\dot{p}$ is

equal to the equivalent plastic rate $\dot{\bar{\varepsilon}}^p$ according to J_2 plasticity.

According to the consistency condition, the differential form of Eq. (8) gives:

$$\dot{f} = \frac{\partial f}{\partial(\mathbf{s}-\boldsymbol{\alpha})} : \dot{\boldsymbol{\sigma}} - \frac{\partial f}{\partial(\mathbf{s}-\boldsymbol{\alpha})} : \dot{\boldsymbol{\alpha}} + \frac{\partial f}{\partial T}\dot{T} \tag{15}$$

Combining Eqs. (7), (11) and (15), the accumulated plastic strain rate can be obtained as:

$$\dot{p} = \frac{2G}{H(T)}\mathbf{N}:\mathbf{D} - \frac{1}{H(T)}(2G\alpha\mathbf{N}:\mathbf{I} + \frac{\partial\sigma_y(T)}{\partial T})\dot{T} \tag{15}$$

where G is shear modulus, H is defined as

$$H = 3G + k_{iso} + k_{kin} \tag{16}$$

where k_{iso} and k_{kin} represent isotropic hardening and kinematic hardening behaviours, respectively, and can be given as

$$k_{iso} = \frac{\partial\sigma_y(T)}{\partial\bar{\varepsilon}^p} \tag{17a}$$

$$k_{kin} = k_{1i}(T) - k_{2i}(T)\mathbf{N}:\boldsymbol{\alpha} \tag{17b}$$

Substituting Eq. (15) into Eq. (7) yields

$$\overset{\circ}{\boldsymbol{\sigma}} = \mathbf{C}^{ep} : (\mathbf{D} - \mathbf{I}\alpha\dot{T}) + \mathbf{C}^{e} : \mathbf{N}\frac{\partial\sigma_y(T)}{H(T)\partial T}\dot{T} \tag{18}$$

where $\mathbf{C}^{ep}$ is elasto-plastic modulus of continuum solids and defined as follows

$$\mathbf{C}^{ep} = \mathbf{C}^{e} - \frac{4G^2}{H}\mathbf{N}\otimes\mathbf{N} \tag{19}$$

2.3. Equation of energy balance

The material system must be in thermodynamic equilibrium. The local form of the first law of thermodynamics can be expressed as

$$\rho c_p\dot{T} = W^{pd} + \rho r - J\cdot div(\mathbf{q}) \tag{20}$$

where $J = \det\mathbf{F}$, c_p is specific heat and it is temperature dependent material parameter. $\mathbf{q}$ is thermal flux tensor, r is the internal thermal source, T is temperature. W^{pd} is the plastic dissipation term.

The latent stored energy for cold worked mild steel and copper was measured [18], which was assumed that the stored energy was a constant fraction of plastic work. However, subsequent experiment [19, 20] show it is dependent on the accumulated strain. Therefore, the heat generation is assumed as the rate of the plastic work multiplied by a function $\eta(p)$ related to calculated plastic strain:

$$W^{pd} = \eta(p)\cdot\boldsymbol{\sigma}:\mathbf{D}^p \tag{21}$$

According to Fourier's law, the heat conduction in the isotropic material can be expressed as

$$\mathbf{q} = -\mathbf{k}\partial_x T \tag{22}$$

The conductivity tensor $\mathbf{k}$ is assumed to be an isotropic tensor, that is related to a scalar material parameter K and $\mathbf{k} = K\mathbf{I}$.

Combining Eqs. (20), (21) and (22), the energy balance equation can be rewritten as

$$\rho c_p \dot{T} = \eta(p) \cdot \boldsymbol{\tau} : \mathbf{D}^p + \rho r + J \cdot div(\mathbf{q}) \tag{23}$$

The general form of three-type thermal boundary conditions are expressed as

$$\mathbf{q} : \mathbf{n} = -q_s\big|_{s1} + h(T_s - T_0)\big|_{s2} \tag{24}$$

$$T\big|_{s3} = T_s \tag{25}$$

These boundary conditions represent specified flux, convection and specified temperature on the respective parts of boundary, s_1-s_3. Here, h is the convection coefficient and $\mathbf{n}$ is the surface normal tensor.

2.4. Solution method

To solve thermo-mechanically coupling problem, coupled method and staggered method can be selected. The coupled method is more realistic even though it is computationally expensive due to involving handling of a large system of equations at every increment, which is necessary when a very large temperature gradient appears in an increment step. The staggered method have been improved to solve thermo-elasto-plastic problem [21], it is numerically convenient because it reduces the computational efforts significantly. In the work, the numerical treatment of coupled finite element analysis is based on the staggered solution scheme. The temperate fields are solved and as a known deformation field to apply in the deformation field, the temperature is updated as a common variable after iterating the two solutions until convergence. Moreover, a finite element implementation into finite element code, i.e., Abaqus, is also necessary for considering the thermal exchange with the around environment in thermo-mechanically coupled structural analysis. Based this purpose, the proposed model is implemented into Abaqus by combining user subroutine UMAT and UMATHT. The heat generation from plastic work is given by the heat generation rate RPL, which is related to plastic work and heat exchange factor η. The deformation and temperature fields are solved simultaneously at a reference temperature.

It is well known that the work done in a close loop is not exactly zero based on the hypoelastic-plastic frame. The stabilization with dissipated energy fraction option in the transient coupled temp-displacement analysis should be used to improve the convergence.

3. Numerical examples

3.1. Uniaxial tension

In this section, a numerical example was provided to simulate typical thermo-mechanically coupling effect. Thermally triggered necking of solid bar has been studied in literature [22], which is considered as a consequence of thermo-mechanically coupling. A 4-node axisymmetric thermally coupled quadrilateral element CAX4HT is used for coupled temperature-displacement analysis, the

finite element mesh is shown in Figure 1(a). To capture the necking process more accurately, a dense mesh is used nearby central section the specimen and ALE mesh technique is applied in the same place. The total length of the bar is 60mm, the length of work segment is 30mm, the radius of transition circular arc is 4mm and the radius of work segment is 4mm. Convection is applied on all free surfaces for a physically realistic simulation, the h is chosen to be 20000Wm^2/^{o}C, which is a generally used value [16]. For rail steel used here [24], the heat exchange factor η and its relation with accumulated plastic strain is not known. And then the factor η is simplified to be a constant value 0.9. For isotropic hardening, b and Q_{sa} are set to 0.25 and 100MPa. The upper end is fixed all freedoms and tensile velocity of 1mm/s is applied in the symmetrical plane. The surrounding temperature is assumed as room temperature 20^{o}C. The maximum allowable temperature change per increment is set to 10^{o}C. Total time 0.4s is used in the simulation and the automatic incrementation is used, the whole solution consist of 314 increment steps. Thermal-mechanical properties of the rail steel for the simulated specimen are given in Table 1. In the most quasi-static tension simulations, the increased temperature generated from plastic work is less than 100^{o}C, and then only part parameters are present here.

The equivalent stress, equivalent plastic strain and temperature were shown in Figure 1 (b), (c) and (d), respectively. It is found that necking can be reproduced successfully without any initial geometrical defect. Moreover, the temperature distribution is consistent with the equivalent plastic strain one, which shows that the temperature change causes by the plastic work. It must be noted that the isothermal analysis gives rise to a classical bifurcation problem, an initial defect must be introduced to trigger necking. However, the thermo-mechanically coupled problem is not a bifurcation problem, since inelastic heat generation gives rise to an increased temperature in the specimen and convection results in the non-homogeneous temperature distribution, which in combination with the thermal softening, triggers necking [23].

Table 1. Thermo-mechanical properties used in simulations [24]

T (℃)	E (GPa)	σ_y (MPa)	v	k_1 (GPa)	k_2	T (℃)	C_p (W/m-℃)	K (J/(Kg.C))	T(℃)	α (1e-6)
24	213	483	0.295	22.7	200	0	59.71	420	0	9.89
230	201	465.1	0.307	21.9	200	350	40.88	630	90	11.3

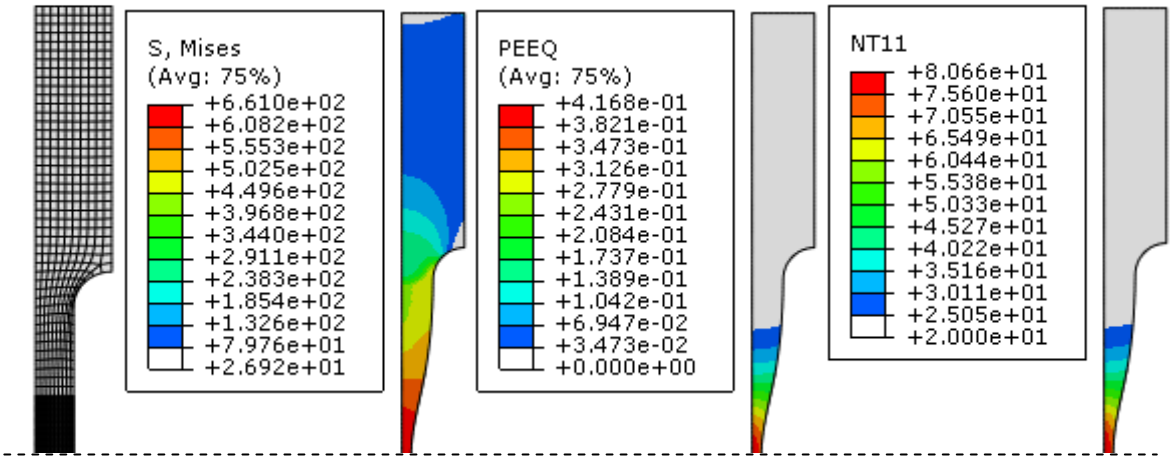

(a) (b) (c) (d)

Figure 1. Finite element simulations for necking of a circular bar with kinematic hardening model at time 0.4s: (a) the axisymmetrical finite element model with a symmetry plane (dot line); (b) the distribution of

equivalent von Mises stress; (c) the distribution of equivalent plastic strain; (d) the distribution of temperature

The thermo-mechanical coupling effect results in a significant thermal softening effect as shown in Figure 2. The load decreases with an increasing displacement when thermal-induced necking occurs. It is noted from Table 1 that the rail steel used in the simulation has a relative hardening parameter, which results in a flat plastic flow when applied displacement is less than 2mm.

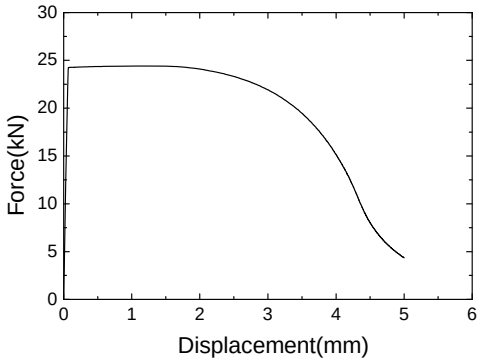

Figure 2. Force-displacement curve

3.2. Cyclic loading

In this example, thermo-mechanically coupling effect is investigated under cyclic stressing. An unsymmetrical stress cycling is applied in the symmetrical plane shown in Figure 1(a) and a total of 30 cycles were calculated. Figures 3(a) and (b) show the stress-strain curves located inside and outside nodes of central section of specimen, respectively. S22 and LE22 are Cauchy stress and logarithmic strain along Y direction, respectively. It is shown that the strain inside node of central section is much more than strain in outside node, which results in a large hysteresis loop in inside node of central section, i.e., more plastic work is done.

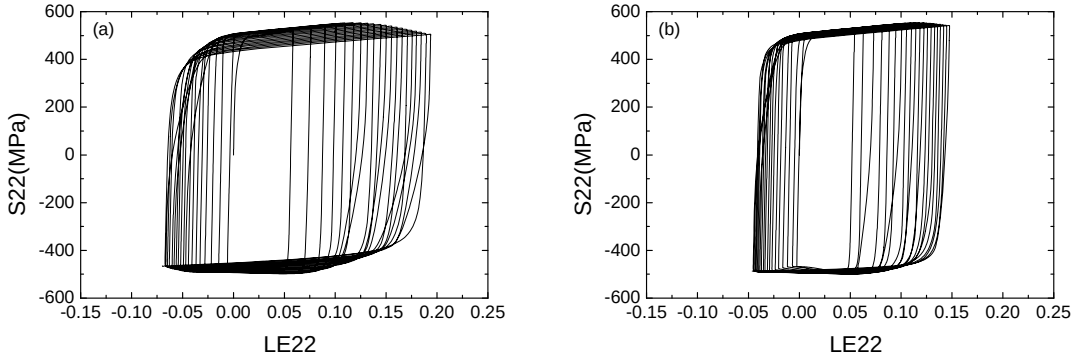

Figure 3. Stress-strain curves along loading direction: (a) inside node in central section; (b) outside node in central section.

Figures 4(a) and (b) show the accumulated plastic strain and temperature for inside and outside nodes in central section, respectively. It is found that more accumulated plastic strain appears in inside than outside nodes of central section. Corresponding, the temperature is higher for inside

node in central section due to conduction and convection. More accumulated plastic strain results in more inelastic heat generation; higher temperature result in more plastic strain due to thermal softening. It is the result the coupling among stress, deformation and temperature.

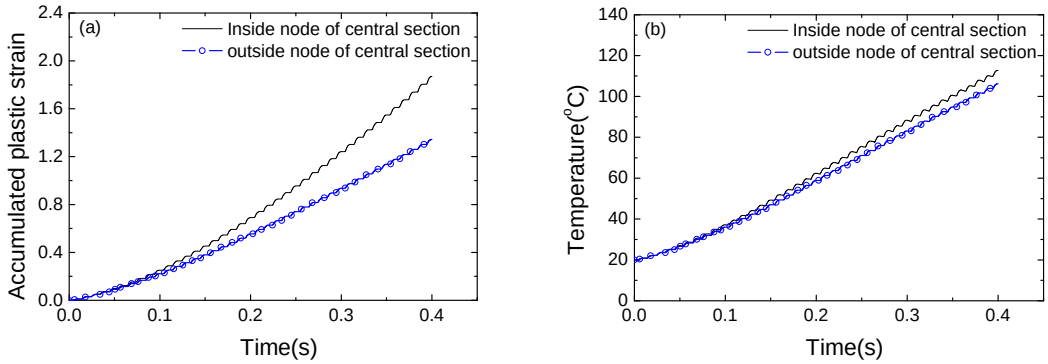

Figure 4. (a) accumulated plastic strain versus time and (b) temperature versus time located in different points.

For rail steel used here [24], the heat exchange factor η and its relation with accumulated plastic strain are not known. However, the influence of the heat exchange factor η on temperature field can be discussed by change the constant value of η, as shown in Figure 5. The total simulated time is limited within 0.1s. It is shown that isotropic hardening contributes more large thermal effect than isotropic hardening when the heat exchange factor η is fixed as 0.9. If only kinematic hardening is considered, the more temperature change occurs with the increased the heat exchange factor η at a fixed time. More important is that the temperature is accumulated with the increased loading cycle. It implies that the inelastic thermal generation can be neglected at a large cyclic number, e.g., low-cycle fatigue, even though the plastic strain is not significantly large.

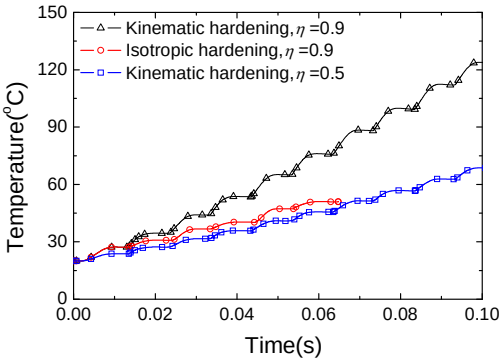

Figure 5. The curves of temperature versus time for isotropic hardening and kinematic hardening with different factors η

4. Conclusions

In the work, a thermo-mechanically coupling cyclic plasticity model with nonlinear isotropic and kinematic hardening was established at large deformations based on hypoelastic-plastic theory. The contribution of plastic dissipation to internal heat generation of materials was also addressed. The temperature dependent mechanical properties are employed. And then, the proposed model is

implemented into Abaqus by combining user subroutine UMAT and UMATHT. Transient coupled temperature-displacement finite element analysis was carried out to investigate thermo-mechanically coupled behaviours under monotonic and cyclic loadings. The thermally induced necking was reproduced without introducing any initial geometrical defect. The inelastic heat generation and, consequently, temperature are accumulated with an increased cyclic number, the interaction between deformation and thermal softening can be neglected, which should be addressed to constructing a more accurate model for predicting ratchetting at large cycles.

Acknowledgements

This work was financially supported by National Natural Science Foundation of China (11025210, 11202171) and the Fundamental Research Funds for the Central Universities (SWJTU12CX044).

References

[1] P.J. Armstrong, C.O. Frederick, A mathematical representation of the multiaxial Bauschinger effect. GEGB report RD/B/N731, Berkeley Nuclear Laboratories, 1966.

[2] J.L. Chaboche, G. Rousselier, On the plastic and viscoplastic constitutive equations. part I and II. J Press Vessel-T ASME 105(1983) 153-164.

[3] N. Ohno, J.D. Wang, Nonlinear kinematic hardening rule with critical state of dynamic recovery, part I: formulation and basic features for ratchetting behavior. Int J Plasticity 9(1993)3575-3590.

[4] M. Abdel-Karim, N. Ohno, Kinematic hardening model suitable for ratchetting with steady state. Int J Plasticity 16 (2000) 225-240.

[5] S. Bari, T. Hassan, Anatomy of coupled constitutive models for ratcheting simulations. Int J Plasticity 16(2000)381-409.

[6] X. Chen, R. Jiao, Modified kinematic hardening rule for multiaxial ratcheing prediction. Int J Plasticity 20(2004) 871-898.

[7] Y.J. Liu, G.Z. Kang, Q. Gao. Stress-based fatigue failure models for uniaxial ratchetting-fatigue interaction, Int J Fatigue 30(2008)1065-1073.

[8] L. Wu, Z.F. Wen, W. Li, X.S. Jin, Thermo-elastic-plastic finite element analysis of wheel-rail sliding contact. Wear 271 (2011) 437-443.

[9] F. Yoshida, T. Uemori, A model of large-strain cyclic plasticity describing the Bauschinger effect and workhardening stagnation. Int J Plasticity 18(2002)661-686.

[10] A.S. Khan, K.M. Jackson, On the evolution of isotropic and kinematic hardening with finite plastic deformation, part I: compression/tension loading of OFHC copper cylinders. Int J Plasticity 15(1999) 1265-1275.

[11] Z. Hu, Work-hardening behavior of mild steel under cyclic deformation at finite strains. Acta Metall. Mater. 42(1994)3481-3491.

[12] G. Jahonsson, M. Ekh, K. Runesson, Computational modeling of inelastic large ratcheting strains. Int. J. Plasticity 21(2005) 955-980.

[13] M. Wallin, M. Risinmaa, N.S. Ottosen, Kinematic hardening in large strain plasticity. Europ. J. Mech A/Solid 22(2003)341-356.

[14] G. Jahonsson, J. Ahlstr o¨m, M. Ekh, Parameter identification and modeling of large ratcheting strains in carbon steel, Comput Struc 84(2006)1002-1011.

[15] H. Xiao, O.T. Bruhns, A. Meyes, Thermodynamic laws and consistent Eulerian formulation of finite elastoplasticity with thermal effects. J Mech Phys Solids 55(2007)338-365.

[16] Y. Tadi Beni , M.R. Movahhedy, Consistent arbitrary Lagrangian Eulerian formulation for large deformation thermo-mechanical analysis, Mater Design 31(2010)3690-3702.
[17] E.H. Lee, Elastic-plastic deformation at finite strains. J Appl Mech 36 (1969)1-6.
[18] G. Taylor, H. Quinney, The latent energy remaining in a metal after cold working. Prog. Mater. Sci. A 143(1934)307-326.
[19] M. Bever, D. Holt, A. Tichener, The stored energy of cold work. Prog Mater Sci (1973)7.
[20] W. Oliferuk, W. Swiatnicki, M. Grabski, Rate of energy storage and microstructure evolution during the tensile deformation fo austenitic steel. Mater Sci Eng A 161(1993)55-63.
[21] P. Rosakis, A. Rosakis, G. Ravichandran, J. Hodowany, A thermodynamic internal variable model for the partition of plastic work into heat and stored energy in metals. J Mech Phys Solids 48(2000)581-607.
[22] J. Simo, F. Armero, Recent advances in the numerical analysis and simulation of thermoplasticity at finite strain. In: D. Besdo, E. Stein, Finite inelastic deformations- Theory and applications. Springer, Berlin, (1992)259-272.
[23] P. Ha˚kansson, M. Wallin, M. Ristinmaa, Comparison of isotropic hardening and kinematic hardening in thermoplasticity. Int J Plastcity 21(2005)1435-1460.
[24] T. Bradon, G. Jeff, A. B. Periman, Investigation of effects of sliding on wheel tread damage, Int Mech Engng Congress Exposition ASME, Nov 5-11, Orlando, Florida USA (2005)1-7.